Fröhlich Mass in GaAs-Based Structures

C. Faugeras,[1] G. Martinez,[1] A. Riedel,[2] R. Hey,[2] K. J. Friedland,[2] and Yu. Bychkov[1,3]

[1]*Grenoble High Magnetic Field Laboratory, MPI-FKF and CNRS, BP 166, 38042 Grenoble CEDEX 9, France*
[2]*Paul Drude Institute, Hausvogteiplatz 5-7, D-10117 Berlin, Germany*
[3]*L.D. Landau Institute for Theoretical Physics, Academy of Sciences of Russia, 117940 Moscow V-334, Russia*
(Received 7 July 2003; published 12 March 2004)

The Fröhlich interaction is one of the main electron-phonon intrinsic interactions in polar materials originating from the coupling of one itinerant electron with the macroscopic electric field generated by any longitudinal optical (LO) phonon. Infrared magnetoabsorption measurements of doped GaAs quantum well structures have been carried out in order to test the concept of Fröhlich interaction and polaron mass in such systems. These new experimental results lead one to question the validity of this concept in a real system.

Based on the Fröhlich interaction, polaronic effects were early studied by Lee and Pines [1] and also by Feynman [2] on theoretical grounds: Simple consequences were derived leading to the concept of the polaron mass, and reproduced in many textbooks [3]. This conceptual interaction also attracted much attention, on the experimental side, in either three- or quasi-two-dimensional (3D or Q2D) semiconductors [4] which were model systems to study the effect. For the simplest case of a Q2D semiconductor, the single-particle energy spectrum of electrons of mass m^*, in a perpendicular magnetic field $B_\perp$, consists of equally spaced ($\hbar\omega_{c\perp} = eB_\perp/m^*$) energy states known as Landau levels labeled with an integer index n going from 0 to infinity: One direct consequence of the polaronic concept is the prediction of the resonant magnetopolaron coupling (RMPC) which anticipates a nonlinear field variation of the cyclotron resonance (CR) energy, $\hbar\omega_c$, when $\hbar\omega_c \simeq \hbar\omega_{LO}$, with a pinning of the CR *above* $\hbar\omega_{LO}$. Such experimental evidence is quite difficult to obtain because the range of energies concerned coincides with that of the strong absorption of the phonon band (Restrahlen) of the material, therefore obscuring the data. The theory itself raises also fundamental questions because, in real materials, one always has many electrons which are known to oscillate in phase as plasmons developing in turn a macroscopic electric field which couples to that of the LO phonon, generating hybrid plasmon-phonon modes. What really happens? Does the polaronic concept remain valid? To our knowledge, there is no quantum mechanical treatment of the hybrid modes and therefore it is difficult to answer these questions on theoretical grounds.

Experiments performed in suitable conditions are, however, able to bring new light to that matter. Overcoming the problem of the Restrahlen band is indeed technically very difficult in 3D semiconductors. In that respect the Q2D structures, grown by molecular beam epitaxy (MBE), are more appealing because, besides the fact that, with the remote doping technique, carriers can remain quasi-free at the lowest temperatures, one can remove by selective chemical etching the whole MBE structure from the substrate (lift-off process). It is then possible to deposit it on an infrared transparent substrate, such as Si for instance, which is wedged with an angle of a few degrees to avoid interference effects. This structure is composed of a single doped GaAs quantum well (QW) of width L and areal density n_S sandwiched between two GaAs-AlAs superlattices with the Si-n-type doping performed symmetrically on both sides of the QW [5]. This enables one to grow structures of quasi-2D electron gas (2DEG) combining high density and high mobility. We already reported results [6] on such a sample with $L = 10$ nm, $n_S = 12 \times 10^{11}$ cm^{-2} [7]. The same process has been applied to new samples with similar structures but with $L = 13$ nm and various lower doping levels. Magnetoinfrared transmission measurements are done in an absolute way for any fixed magnetic field B: This is achieved with a rotating sample holder allowing one to measure reference spectra in the same conditions on a parent wedged piece of Si substrate. With the $\vec{k}$ vector of the incoming light parallel to $\vec{B}$, the growth axis of the sample was maintained either parallel to this direction [perpendicular Faraday (PF) configuration] or tilted by an angle θ with respect to it [tilted Faraday (TF) configuration]. The light was guided through an oversized guide pipe ending by a cone to minimize the divergence of the beam. The interpretation of the experimental results is done by comparing them with a simulation of the multilayer transmission by an appropriate model. This is essential because, in the frequency range of interest, the spectra can be distorted by dielectric interference effects independent of any specific electron-phonon interaction.

The previous study [6] reported on PF configuration measurements where no sign of RMPC was observed. This was not necessarily a proof that the effect was not existing because it could have been screened by the high value of n_S: Indeed theoretical simulations [8], including the RMPC, of data obtained with such high density QW

were still showing a small interaction. New experiments with a lower n_S, for which this simulation provided clear effects, were necessary to check the concept of the RMPC. The doping level of the new lift-off samples ranged between $n_S = 7.0 \times 10^{11}$ cm^{-2} (sample 1200) and $n_S = 9.0 \times 10^{11}$ cm^{-2} (sample 1211) with respective mobilities of $\mu_{dc} = 260$ (m^2/V)/s and $\mu_{dc} = 280$ (m^2/V)/s [7]. All experimental results reported here have been obtained at a fixed temperature of 1.8 K. We will concentrate on the results obtained for $B_\perp$ around 20 T for which the CR span the Restrahlen band of GaAs. For both samples, in that range of fields, the filling factor of the structure $\nu = n_S h/(eB)$ remains essentially lower than 2 and, in that case, nonparabolicity (NP) effects can be ignored.

Typical spectra, for sample 1200, are displayed in Fig. 1. The absolute transmission (AT) at $B = 0$ T and $\theta = 60°$ is shown in Fig. 1(a). The strong absorption features are those related to the TO phonons of GaAs and AlAs, whereas the weak ones are those related to the LO modes which are known to become active in absorption for thin slabs [9] in the TF configuration. They clearly originate from the layers of the superlattices surrounding the doped QW. They are slab modes and give a lower bound of the energy of LO modes in the whole structure. In Fig. 1(b), the absolute transmission of the sample in a TF configuration is displayed for $\theta = 20°$ and $B_\perp = 20.7$ T. In practice with the available magnetic fields, we are led to work with angles where the LO

phonons are less visible but they are still clearly present as indicated by the vertical dashed lines. Two CR transitions, labeled CR1 and CR2 (vertical dotted lines), are now present, the CR2 feature being, for that field, at a *lower* energy than $\hbar\omega_{LO}$ (GaAs). In Fig. 1(c), we show the relative transmission (RT) obtained by dividing the AT spectrum of Fig. 1(b) by the AT spectrum at $B = 0$ T for the same angle. The RT spectra are a combination of four experimental ones and therefore the noise is more important. However, the only remaining features are those related to the contribution of the 2DEG. The energies of the CR1 and CR2 structures for each sample, traced as a function of $B_\perp$, are displayed in Fig. 2 for different angles. Whereas in the PF configuration (empty black squares) no sign of interaction is observed, in the TF configuration a pronounced anticrossing of the CR1 and CR2 components occurs, which increases with θ, one of the components remaining pinned at an energy of 35.6 ± 0.05 meV for the sample 1200 and 35.5 ± 0.05 meV for the sample 1211, both energies being lower than $\hbar\omega_{LO}$

FIG. 1 (color). Experimental transmission spectra (empty dots) of sample 1200. (a) Absolute transmission for $B = 0$ T and $\theta = 60°$. (b),(c) Absolute transmission and relative transmission, respectively, for $B_\perp = 20.7$ T and $\theta = 20°$. The continuous red curves are the fit of data with the model described in the text.
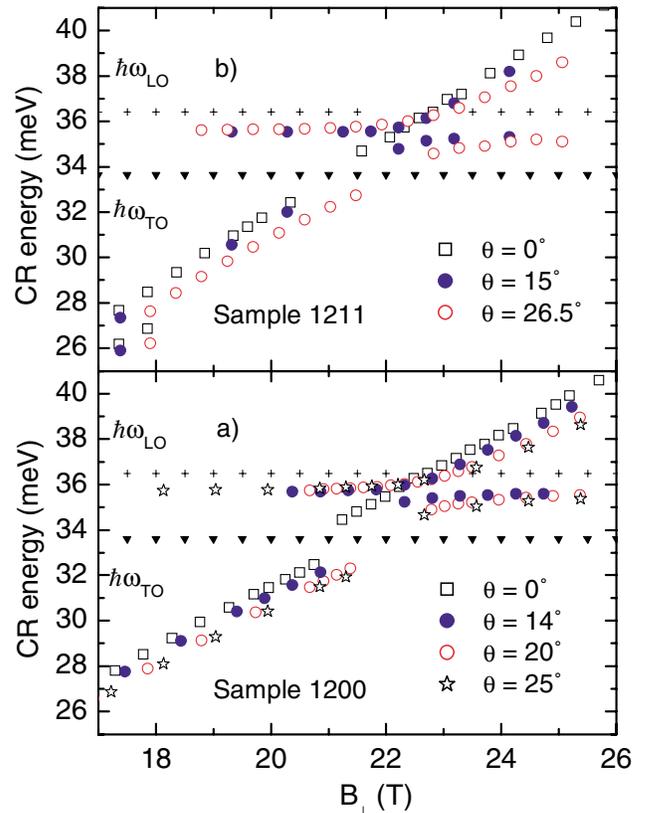
FIG. 2 (color). Observed cyclotron energies for sample 1200 (a) and sample 1211 (b) for different tilt angles. The crosses and black down triangles are the measured LO and TO energies, respectively, and the empty squares the cyclotron energies in the PF configuration. Other points are the observed CR energies in the TF configuration: (a) full dots, $\theta = 14°$; empty dots, $\theta = 20°$; stars, $\theta = 25°$; (b) full dots, $\theta = 15°$; empty dots, $\theta = 26.5°$. Results in (b) for $B_\perp$ lower than 18 T correspond to filling factors > 2 when nonparabolicity effects are apparent.

(GaAs). Other samples with different densities of electrons ($n_S = 5.8 \times 10^{11}$ cm^{-2} and $n_S = 8.8 \times 10^{11}$ cm^{-2} and the same L of 13 nm or with a smaller L of 10 nm and $n_S = 12 \times 10^{11}$ cm^{-2}) have also been investigated and demonstrate exactly the same qualitative features.

To interpret these results, one has to calculate the transmission of the whole structure. This requires a full derivation of the multilayer structure transmission in the TF configuration, a rather complicated problem which we have succeeded to solve in some specific cases and which will be detailed in a further publication [10]. We just here outline the principles. We used a standard approach which consists of evaluating for each layer N, with a dielectric tensor $\overleftrightarrow{\varepsilon}_N(\omega)$, the transfer matrix M_N after finding the appropriate modes of propagation of light $\vec{k}_N^i$ inside the layer, by solving the Maxwell equations. Taking the z axis perpendicular to the layer, and defining the y-z plane as the plane of incidence which also contains $\vec{B}$, the angle θ is defined as the angle $(\vec{z}, \vec{B})$. There are four modes $k_{z,N}^i$ for each layer. The 4×4 transfer matrix is built by writing the conservation of the tangential components of the electric and magnetic fields of the light at each interface of the layer. If $\overleftrightarrow{\varepsilon}_N(\omega)$ is diagonal, as in layers which do not contain free electrons (or at $B = 0$ T), the transfer matrix decomposes into two blocks of 2×2 matrices related to the TE and TM modes, respectively. This result is well known and has been used [11] to measure the LO phonon frequencies of semiconductors in a way similar to the results reproduced in Fig. 1(a). For the doped QW, in the TF configuration, all elements of $\overleftrightarrow{\varepsilon}_{QW}(\omega)$ and therefore of the transfer matrix are nonzero and the TE and TM modes are mixed. The resulting total transfer matrix has the same properties, and a special treatment [10] needs to be developed to extract the transmission of the structure. This can be done as soon as the dielectric tensor of the QW in the TF configuration has been defined.

In the PF configuration, for any finite value of B, the z part of the 2DEG wave function is decoupled from the x-y part. When $\theta \neq 0$, this decoupling is no longer valid and, as we shall see below, is indeed responsible for the observed anticrossing. One has then to reproduce the mixing of the z and the x-y parts of the 2DEG wave function with the best accuracy. For the square QW which is under study, this mixing can be evaluated only in perturbation theory [12]. On the other hand, if we assume the z-confining potential to be parabolic, with a characteristic energy $\hbar\Omega$ separating the electric subbands, the coupling can be evaluated analytically at all orders. Of course, the strength of the coupling is modified, the dipole oscillator strengths along the z axis being different between a square QW and a parabolic one. It is this model, based on the Drude formalism, that we have used to evaluate, neglecting retardation effects, all components of $\overleftrightarrow{\varepsilon}_{QW}(\omega)$ and then simulate the transmission. Before discussing these simulations it is instructive to look at the structure of two characteristic components of $\overleftrightarrow{\varepsilon}_{QW}(\omega)$. The real parts of ε_{xx} and ε_{zz} are expressed, ignoring

damping effects, as [10]

$$\varepsilon_{xx} = \varepsilon_L - \frac{\omega_p^2(\omega^2 - \Omega^2)}{(\omega^2 - \omega_1^2)(\omega^2 - \omega_2^2)}, \qquad (1)$$

$$\varepsilon_{zz} = \varepsilon_L - \frac{\omega_p^2(\omega^2 - \omega_{c\perp}^2)}{(\omega^2 - \omega_1^2)(\omega^2 - \omega_2^2)}, \qquad (2)$$

where ε_L is the contribution of the lattice, $\omega_p^2 = 4\pi e^2 n_S/(Lm^*)$ the square of the plasma frequency, and ω_1^2 and ω_2^2 are the solutions of the equation:

$$\omega^4 - (\Omega^2 + \omega_c^2)\omega^2 + \omega_{c\perp}^2\Omega^2 = 0, \qquad (3)$$

with $\omega_c = eB/(\hbar m^*)$. When $\Omega \gg \omega_{c\perp}$, $\omega_1 \to \omega_{c\perp}$ and $\omega_2 \to \Omega$. In the present case, however, the exact values for the poles are introduced in the calculation. This explains why, in Fig. 2, far from the anticrossing region the energies of the CR lines do not coincide with the values obtained in the PF configuration.

Different fitting steps have to be performed. We first have to fit ε_L with standard values as already done [6] and shown in Fig. 1(a) (red continuous lines). In fact, in the region of $\hbar\omega_{TO}$ (GaAs), interference effects between phonon and CR absorptions become important, and this is the reason why we prefer to interpret the relative transmission spectra [Figs. 1(c) and 3] for which these spurious effects are minimized. They are, however, not eliminated and, for this reason, we ignore in the fitting process a region of ± 0.5 meV around $\hbar\omega_{TO}$ (GaAs), sketched as the hatched region in Fig. 3. In this figure, experimental data (empty dots) and their simulations (red continuous curves) for sample 1200 are displayed for $\theta = 25°$. There are different fitting parameters to adjust: n_S, m^*, τ_{CR}, Ω, and θ, τ_{CR} being the scattering time entering the Drude model. In the PF configuration, n_S is fitted at lower fields with the model extended for NP effects [10] together with m^* and τ_{CR}. Outside the energy region around $\hbar\omega_{TO}$ (GaAs) where there are signs of some interaction (at least for the sample 1200) which are not discussed here, the values of m^* fitted correspond quite well to the expected variation induced by NP effects [13], whereas the mobility $\mu_{CR} = e\tau_{CR}/m^*$ ranges around 150 (m^2/V)/s revealing the good quality of the samples. The angle θ has also to be fitted because, for technical reasons, the Si substrate being wedged, θ can differ by a few degrees from the mechanical angle. It is fitted by setting the m^* value constant for a given value of $B_\perp$. This is not completely independent of the value of Ω but the loop easily converges. The values of $B_\perp$ indicated in the figures are calculated values of $B \times \cos(\theta)$. Finally, Ω is fitted in such a way the splitting of the CR1-CR2 lines can be best reproduced. We impose also, in the fitting process, the value of Ω to be constant for all angles and QW having the same width L. As an example, the results, shown in Fig. 3 for sample 1200, are obtained for a value of $\Omega = 63$ meV (with an uncertainty of ± 3 meV). These results clearly demonstrate the anticrossing features observed
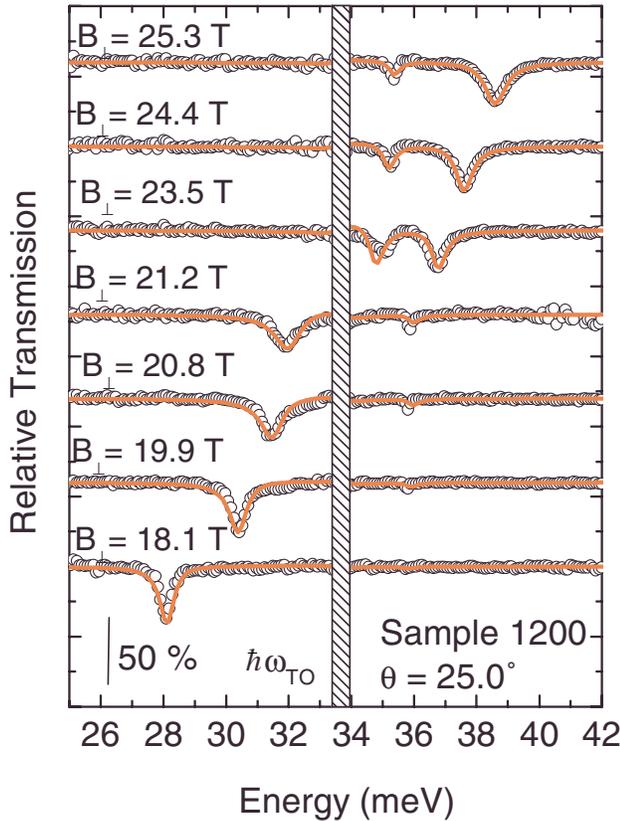
FIG. 3 (color). Fit of the relative transmission curves for sample 1200 at $\theta = 25°$. The curves are shifted for clarity. Empty dots are experimental points and full continuous curves the corresponding calculated relative transmission spectra. The hatched region corresponds to that of $\hbar\omega_{TO}$ (GaAs) (see text).

experimentally. The fit reveals some slight deficiency which is sample dependent but the overall agreement is surprisingly good. It is interesting to note that if one calculates, at $B = 0$ T, the zeros of ε_{zz} [Eq. (2)] with the fitted value of Ω, one finds for the low energy modes 35.62 meV for the sample 1200 and 35.49 meV for the sample 1211, values which agree very well with the experimental findings. These modes are the so-called plasmon-phonon-intersubband (PPI) modes [14]. Therefore the observed anticrossing occurs between the CR mode and this hybrid PPI mode. They are coupled by symmetry but not by any *specific electron-phonon interaction*. We think, although it is approximate, the model keeps all the physical and symmetry aspects of the problem. One direct consequence is that, when Ω increases, the oscillator strength of the PPI-like mode rapidly decreases to zero [10]. Therefore, for a pure 2DEG, there is no longer any interaction whatever the angle. The data in the PF and TF configurations do not show any sign of interaction related to the Fröhlich coupling: We are therefore led to conclude that the concept of polaronic mass, related to this interaction, is no longer effective.

All the discussion is based on the assumption that we are dealing with carriers for which a plasma frequency

can be defined. It is known that, for bound electrons, such as the ones found in neutral shallow impurities, the $1s$-$2p^{+}$ absorption reveals [15] the Fröhlich interaction around the energy of the LO phonon in GaAs, but then the mass of such an electron is not defined. The same situation holds for electrons in quantum dots [16]. It is also true that there is still some electron-phonon interaction present in such a system: Indeed, around the TO frequency, there is a clear sign of interaction especially in sample 1200. This is an interaction which may be driven by the mechanism of a deformation potential which is at the origin, for instance, of the Raman response of such structures.

In conclusion, we have performed careful magneto-optical measurements of the infrared absorption related to quasi-two-dimensional electron gas, with different densities, in a range of magnetic fields which allows the cyclotron resonance to span the optical range of phonon energies. All singularities observed can be explained quantitatively without any electron-phonon coupling of the Fröhlich type. We argue that this supports the idea that the concept of the Fröhlich polaron mass has to be reexamined in a real material.

[1] T. D. Lee and D. Pines, Phys. Rev. **92**, 883 (1953).
[2] R. P. Feynman, Phys. Rev. **97**, 660 (1955).
[3] C. Kittel, *Quantum Theory of Solids* (Wiley, New York, 1963), pp. 130–142.
[4] For a review, see, e.g., J. T. Devreese, *Polarons in Ionic Crystals and Polar Semiconductors* (North-Holland, Amsterdam, 1972).
[5] K. J. Friedland *et al.*, Phys. Rev. Lett. **77**, 4616 (1996).
[6] A. J. L. Poulter *et al.*, Phys. Rev. Lett. **86**, 336 (2001).
[7] The carrier densities reported in this Letter, for all samples, are obtained from the fit of data with the model detailed in the following including nonparabolicity effects. They are systematically lower by (6–8)% with respect to the value obtained from transport data on the parent non-lift-off sample. The values of mobilities given here are, however, those obtained from these data.
[8] X. G. Wu *et al.*, Phys. Rev. Lett. **84**, 4934 (2000).
[9] D. W. Berreman, Phys. Rev. **130**, 2193 (1963).
[10] Yu. Bychkov *et al.* (to be published).
[11] M. D. Sciacca *et al.*, Phys. Rev. B **51**, 7744 (1995).
[12] See, for instance, G. Bastard, *Wave Mechanics Applied to Semiconductor Heterostructures* (Les éditions de Physique, Paris, 1992).
[13] C. Hermann and C. Weisbuch, Phys. Rev. B **15**, 823 (1977).
[14] A. Pinczuk *et al.*, Solid State Commun. **36**, 43 (1980).
[15] S. Huant *et al.*, Europhys. Lett. **7**, 159 (1988).
[16] S. Hameau *et al.*, Phys. Rev. Lett. **83**, 4152 (1999).